UC Berkeley
UC Berkeley Previously Published Works

Title

Transcriptomic contributions to a modern cytoarchitectonic parcellation of the human cerebral cortex

Permalink

https://escholarship.org/uc/item/2z15h3zg

Authors

King, Leana

Weiner, Kevin S

Publication Date

2024-03-16

DOI

10.1007/s00429-023-02754-4

Transcriptomic contributions to a modern cytoarchitectonic parcellation of the human cerebral cortex

Authors

Leana King[1], Kevin S. Weiner[1,2]

1. Helen Wills Neuroscience Institute, University of California Berkeley, Berkeley, California, 94720, United States of America

2. Psychology Department, University of California Berkeley, Berkeley, California, 94720, United States of America

Address correspondence to Leana King. Email: leana.king@berkeley.edu

Abstract

Transcriptomic contributions to the anatomical, functional, and network layout of the human cerebral cortex (HCC) has become a major interest in cognitive and systems neuroscience. Here, we tested if transcriptomic differences support a modern, algorithmic cytoarchitectonic parcellation of HCC. Using a data-driven approach, we identified a sparse subset of genes that differentially contributed to the cytoarchitectonic parcellation of HCC. A combined metric of cortical thickness and myelination (CT/M ratio), as well as cell density, correlated with gene expression. Enrichment analyses showed that genes specific to the cytoarchitectonic parcellation of the HCC were related to molecular functions such as transmembrane transport and ion channel activity. Together, the relationship between transcriptomics and cytoarchitecture bridges the gap among i) gradients at the macroscale (including thickness and myelination), ii) areas at the meso-scale, and iii) cell density at the microscale, as well as supports the recently proposed cortical spectrum theory and structural model.

Key words: cortical thickness, cytoarchitecture, gradation, myelination, transcriptomics

Introduction

Transcriptomic contributions to the anatomical, functional, and network layout of the human cerebral cortex (HCC) has become a major interest in both cognitive and systems neuroscience in the last decade (Fornito et al. 2019; Deco et al. 2021; Arnatkeviciute et al. 2021c; Wagstyl et al. 2022). Recent research shows that active transcription of a small set of genes contributes to large-scale gradients and functional hierarchies across the HCC, which likely contribute to the regional functional and structural differences in the HCC. Specifically, previous findings show that a subset of genes increase or decrease their expression from primary to association cortices (Burt et al. 2018), likely also contributing to the hierarchical organization of functional processing streams (Gomez et al. 2019). Nevertheless, it is largely unknown if transcriptional differences also contribute to modern, algorithmic definitions of cytoarchitectonic areas across the whole HCC (Amunts et al. 2020).

This gap in knowledge persists for at least three main reasons. First, advancements in sequencing methodologies were only developed recently and freely shared with the larger neuroscience and human brain mapping fields, which enables novel links between gene expression in human postmortem tissue to current in-vivo measures of cortical anatomy and function (Hawrylycz et al. 2012; Bludau et al. 2018; Arnatkeviciute et al. 2019; Wang et al. 2022). Second, most human research that has linked transcriptomics to brain-wide features have focused on either connectivity (Arnatkeviciute et al. 2021b; Oldham et al. 2022), functional differentiation (Burt et al., 2018), or a small subset of cortical areas (Zachlod et al. 2022). Third, a modern, observer-independent cytoarchitectonic parcellation of the HCC was only recently published in the last three years. For example, classic cytoarchitectonic approaches (Brodmann 1909; von Economo and Koskinas 1925) rely on the eyes of the

anatomists to qualitatively determine when two adjacent pieces of cortex are cytoarchitectonically distinct. These classic maps still used in cognitive and systems neuroscience have additional flaws aside from their qualitative nature. For example, while 60-70% of HCC is buried in indentations, or sulci (Welker 1990; Armstrong et al. 1995), Brodmann did not examine sulci, despite the fact that thousands of studies continue to cite his map (Abbott 2003; Zilles and Amunts 2010; Zilles 2018). Contrary to these classic approaches, recent methods use observer-independent algorithms to statistically determine a cytoarchitectonic boundary between adjacent pieces of cortex.

Importantly, the modern cytoarchitectonic parcellation of the HCC is functionally meaningful at both the areal and network level. Determining if transcriptomic differences contribute to a modern cytoarchitectonic parcellation of the HCC can guide the broad fields of cognitive and systems neuroscience in understanding the complex relationship among gene expression, cytoarchitecture, and functional networks of the HCC, in addition to targeting genes that could be impacted in deficits altering this multimodal and multiscale relationship (Seidlitz et al. 2020; Arnatkeviciute et al. 2021a).

To address this gap in knowledge, we integrated transcriptional data and cytoarchitectonic parcellations of the HCC from two freely available datasets (Hawrylycz et al. 2012; Amunts et al. 2020). Using a data-driven approach, we identified a sparse subset of genes that differentially contributed to the cytoarchitectonic parcellation of the HCC. These genes were located in two distinct clusters of opposing expression. Interestingly, these clusters were also correlated with a metric that considered the ratio between cortical thickness and myelination. Further analyses of cytoarchitectonic areas revealed both within-network and between-network relationships. When repeating our analyses with a recent multimodal

parcellation of the HCC (Glasser et al. 2016), ~90% of genes were shared between both parcellations, while ~10% were specific to each parcellation. Enrichment analyses showed that genes specific to the cytoarchitectonic parcellation of the HCC were related to molecular functions such as transmembrane transport activity and ion channel activity, while genes specific to the multimodal parcellation of the HCC were related to calcium channel activity and cellular processes such as neuron development. Altogether, our results identify a relationship between genetic expression and an observer-independent cytoarchitectonic parcellation of the HCC, as well as identify novel genes for future studies interested in further understanding the contribution of genetic expression to different anatomical, functional, and multimodal parcellations of the HCC.

Materials and Methods

Text in sections *JüBrain cytoarchitectonic atlas, Allen Human Brain Atlas (AHBA) processing, HCP measure of T1, T2, and cortical thickness* have been adapted from previously described methods in Gomez et al., 2019. Additionally, text in *Gene ontology analyses* has also been adapted from the methods section in Gomez et al., 2021.

Data

1. JüBrain: https://www.fz-juelich.de/inm/inm-1/EN/Home/home_node.html

2. Allen Human Brain Atlas (AHBA): http://brain-map.org/

3. Human Connectome Project (HCP):

https://www.humanconnectome.org/study/hcp-young-adult

4. Von Economo - Koskinas Atlas:

http://www.dutchconnectomelab.nl/economo/

JüBrain cytoarchitectonic atlas

The JüBrain atlas contains cytoarchitectonic areas that have been delineated using an observer-independent statistical approach in 10 human post-mortem brains. 142 areas are included in the present version of the atlas (v2.9), 111 of which are located across the HCC covering roughly 70% of the cortex (Fig. 1a) with 5 cortical gap maps (Supplemental Fig. 1) resulting in full coverage of the HCC (Amunts et al. 2020). These 111 cytoarchitectonic regions have been aligned to both the MNI305 (Colin 27) and MNI152 template space. Given that the AHBA data is also provided in the MNI152 nonlinear asymmetric space, the MNI ICBM 152 (2009c Nonlinear Asymmetric) projection of the cROIs was used.

Geodesic distance

In order to calculate the distance between cROIs, the JüBrain parcellation was converted to a 32,000 vertex mesh surface so that the Connectome Workbench software (Marcus et al. 2011) could be applied. This required first transforming the parcellation from the MNI152 volume space to the fsaverage surface and then, the 32k_fs_LR surface. Once the parcellation was transformed to the appropriate surface, the *cortex* function was used to calculate the geodesic distance along the surface mesh between parcels represented in millimeters (mm). For analyses described below, the pairwise distances between regions were normalized between 0 and 1 with 0 being the absolute shortest distance between any region pair and 1 being the greatest possible distance.

Allen Human Brain Atlas (AHBA) Processing

The gene expression data are from 6 post-mortem human brains and each tissue sample

has been mapped to a set of 3-D coordinates in MNI152 space. The methods for collection, quality control, pre-processing, and normalization of the gene expression data have been described previously (http://help.brain-map.org/display/humanbrain/documentation/). Here, we detail additional pre-processing steps implemented in the present study.

The raw microarray expression data for each of the six donor brains included the expression level of 29,131 genes profiled via 58,692 microarray probes. These data were preprocessed and simultaneously aligned to the JüBrain parcellation by using the abagen package (Markello et al. 2021), which is a Python toolbox that provides a reproducible pipeline processing the transcriptomic data provided by the AHBA. While the package provides several different options across the different processing steps, the default parameters were used as recommended by (Markello et al. 2021), which are briefly described as follows. The first step involves removing probes whose intensity value does not exceed that of background noise and, if there are multiple probes present for a single gene, selecting the probe with the highest differential stability across donors. The next step matches the tissue samples to cROIs and then normalizes expression values for each sample across genes and for each gene across samples across each donor. The scaled robust sigmoid function was used for each normalization step. Lastly, the normalized samples were aggregated into the cROIs as the "get_expression_data" function outputs the dataframe yielding the normalized expression value for each gene within each cROI, resulting in a dataframe of 111 cROIs by 15,630 genes.

Gene Selection

Of the genes that survived quality control implemented via the abagen package, we then sought to identify genes that were most differentially expressed across the cortex. This was done by applying PCA to the cROI expression array, which resulted in a score value for each

cROI provided by the first PC (Fig. 3a). To select for genes of interest, we then selected the genes with the highest absolute feature weight values for PC1. To further remove genes not of interest, the data were filtered to only include 'brain-specific genes' as identified by Burt et al., (2018). Afterwards, the top 200, roughly 1% of the original dataset, most significantly correlated genes were identified (Fig. 1c). Hierarchical clustering was done on the top and bottom 1% of genes based on their expression values across all cROIs to further demonstrate the transcriptomic distinctiveness of these selected 200 genes (Fig. 2a). Additionally, the two expression gradients are visualized in Fig. 2b.

Examining spatial autocorrelation

To identify any trends of spatial autocorrelation in our data, we correlated gene expression profiles between all region pairs using the 15,630 genes that survived pre-processing and plotted each pairwise Pearson's correlation as a function of normalized geodesic distance between the two regions (Supplemental Fig. 3a). Linear regression was performed to generate a model of spatial autocorrelation in the data ($y = -0.6723x + 0.3429$, mean squared error (MSE) = 0.07). Then, in order to compare spatial autocorrelation in this subset of data to the top 200 DE genes, we performed the same correlation, but only using the expression of these 200 genes, which is plotted in Supplementary Fig. 3b as a function of geodesic distance. The MSE of these data was then calculated using the same linear model previously described. As the MSE was much higher (0.29 vs. 0.07) around the autocorrelation fit when using the data from the top 200 DE genes compared to all genes indicates much greater variance in the observed correlations. This suggests that variations in gene expression (N=200) are broadly not due to similar changes in distance between regions.

Hierarchical clustering of cytoarchitectonic regions

To further probe the relationship between variations in gene expression and cytoarchitectonic organization, we implemented a hierarchical clustering algorithm to determine the organization of cROIs based on their differential gene expression. Using the final processed gene expression array (200 DE genes x 111 cROIs), this matrix served as the input to the hierarchical analysis using Euclidean distances and the Ward variance minimization algorithm. This analysis was executed using the clustering linkage function from the Python 'SciPy' package. Results of this analysis can be seen in Fig. 3b, resulting in two clusters at the highest level.

Multimodal Parcellation

To test if the identified genes were specific to the cytoarchitectonic parcellation of the HCC or generalized to additional parcellations of the HCC, we repeated our analyses with a multimodal parcellation of the HCC (Glasser et al., 2016; Fig. 4). To do so, AHBA data were aligned to this multimodal atlas of the HCC using the same process described above for alignment to the cytoarchitectonic parcellation of the HCC. This was done using the abagen package with the same parameters resulting in a normalized expression array of 178 multimodal ROIs by 15,630 genes. The same analyses (*gene selection* and *exploring the relationship of gene expression among ROIs*) were then performed on the multimodal expression array.

HCP measure of T1, T2, and cortical thickness

Group average cortical maps of T1w/T2w ratio maps (which are a proxy for myelination) and cortical thickness were obtained from 1,096 participants included in the

Human Connectome Project (Glasser et al., 2013). In each participant, T1w and T2w scans were collected using 3 Tesla (3T) MRI and then aligned to the fsLR_32k mesh surface where the average values for both T1/T2 and cortical thickness were taken at each vertex as in our previous work (Gomez et al. 2019).

Given that the average anatomical maps were in the HCP fsLR_space, cROI MNI coordinates were transformed into the fsLR space, which was done using Freesurfer (Fischl et al. 1999; Fischl 2012) by applying a transformation to each cROI's surface label. Distribution of values for both measurements within each cROI can be seen in Supplemental Fig. 5. Four cROIs (Area 33, p24ab, s24, and Area 25) displayed a high degree of variability in both HCP measurements and thus, were excluded from future analyses. After cROIs were aligned to the average HCP fsLR surface, we then extracted the mean myelination and cortical thickness value within each cROI along with the standard deviation as in our previous work (Gomez et al., 2019).

We then calculated the ratio between myelination and cortical thickness values as in our previous work (Willbrand et al. 2022). Furthermore, we quantified the relationship between PC scores and the CT/M ratio in two ways: 1) using a linear regression and 2) the correlation between the cROIs PC1 score and mean anatomical value (Fig. 5a). This was also done separately for cortical thickness and myelination (Supplemental Fig. 6). However, given that the CT/M ratio has a stronger correlation with the PC score of cROIs than each metric individually, the CT/M ratio was used as a parsimonious metric related to transcriptomic variation across the HCC. Individual AHBA donor correlations to the HCP-derived CT/M ratio is included in Supplemental Fig. 7.

Von Economo - Koskinas measure of cell density

Histological measurements of cellular density across the cortical mantle and layer-specific measurements of cortical thickness were obtained from the digitized version of the von Economo and Koskinas atlas (von Economo and Koskinas 1925; Scholtens et al. 2018). The atlas contains 48 distinct cortical regions with measurements of morphological information on neuronal count, neuron size, and thickness for each cortical layer and across the whole mantle. The atlas has recently been translated into a digital version that is compatible well with FreeSurfer and has been made publicly available (Scholtens et al. 2018). To obtain the Von Economo - Koskinas measurements per cROI, the two atlases were combined in the same MNI152 (2009c Nonlinear Asymmetric) volume space. Then, for each cROI with its corresponding voxels in MNI space, the same voxels were indexed in the Von Economo atlas and the values were averaged across all the voxels selected. This means that the Von Economo measurements were indexed via cROI voxel location agnostic to the volumetric location of Von Economo regions in which one cROI can have measurements from multiple Von Economo regions. This process was repeated for each morphological measurement. This resulted in an array of 35 different measurements for each cROI: layers 1-6 and overall for cell density, cell size, overall thickness, wall thickness, and dome thickness. Here, we considered the relationship between overall cell density across layers and layer IV thickness (both measurements normalized) to the primary axis of transcriptomic variation (Fig. 5b and c). See Supplementary Fig. 8 for all other regression plots with each variable and each layer.

Gene ontology analyses

To further elucidate the functional characteristics of the different, as well as overlapping, sets of genes identified from our analyses examining the relationship between i) transcriptomics and a cytoarchitectonic parcellation of the HCC and ii) transcriptomics and a

multimodal parcellation of the HCC, we performed three different enrichment analyses using the following open-sourced program: ToppFun within the ToppGene Suite (Chen et al. 2009); https://toppgene.cchmc.org/enrichment.jsp. This open-sourced program detects if any genes exist within the identified set significantly higher than what would be expected by random chance (corrected significance values using a Benjamini-Hochberg False Discovery Rate procedure). For determining if a particular gene group was significant, we chose a p value method of probability density function, and restricted our gene ontology identification to the following three categories: (i) GO: Molecular Function, (ii) GO: Biological Process, (iii) GO: Cellular Component. Importantly, choosing a different p value method (cumulative distribution function), did not significantly change the results. The first enrichment analysis focused on the genes that overlapped between the cytoarchitectonic and multimodal parcellation (Fig. 6a), while the second and third enrichment analyses focused on genes that were unique to either the cytoarchitectonic parcellation or the multimodal parcellation (Fig. 6b).

Results

A sparse subset of brain-specific genes contributes to a modern cytoarchitectonic parcellation of the human cerebral cortex (HCC)

To identify genes that potentially contribute to an algorithmic, observer-independent cytoarchitectonic parcellation of the HCC (Fig. 1a), we assessed gene expression profiles that were significantly different among cytoarchitectonic areas (cROIs) using two freely available datasets: 1) a modern cytoarchitectonic parcellation of the HCC from 10 post-mortem brains (JüBrain: https://www.fz-juelich.de/inm/inm-1/EN/Home/home_node.html) and 2) the Allen

Human Brain Atlas, which consists of transcriptomic data from tissue samples in 6 post-mortem brains (AHBA: http://brain-map.org/). To test if there is a relationship between genetic expression and the observer-independent cytoarchitectonic parcellation of the HCC, transcriptomic data were pre-processed and aligned to the cytoarchitectonic parcellation (Fig.1b) via the abagen package. This process precisely aligned the expression of 15,630 genes (controlling for false positives, duplicate probes, etc; Materials and Methods) across 111 cROIs.

A Principal Components Analysis (PCA) was implemented to identify genes that were most differentially expressed across all 111 cROIs. A histogram (Fig. 1c) of resultant feature weights for each gene empirically supported that a majority of the genes do not contribute to the primary axis of transcriptomic variation. In order to identify genes that most strongly contributed to the cytoarchitectonic arealization of HCC, we restricted our analyses to the top 1% (n=200) genes that were most differentially expressed as in our previous work (Gomez et al. 2019, 2021) and were 'brain-specific' (as identified by Burt et al., 2018) (Fig. 1c, light purple). Importantly, variation in expression of the identified genes across the geodesic surface were not driven by trends in spatial autocorrelation (Supplementary Fig. 3b).
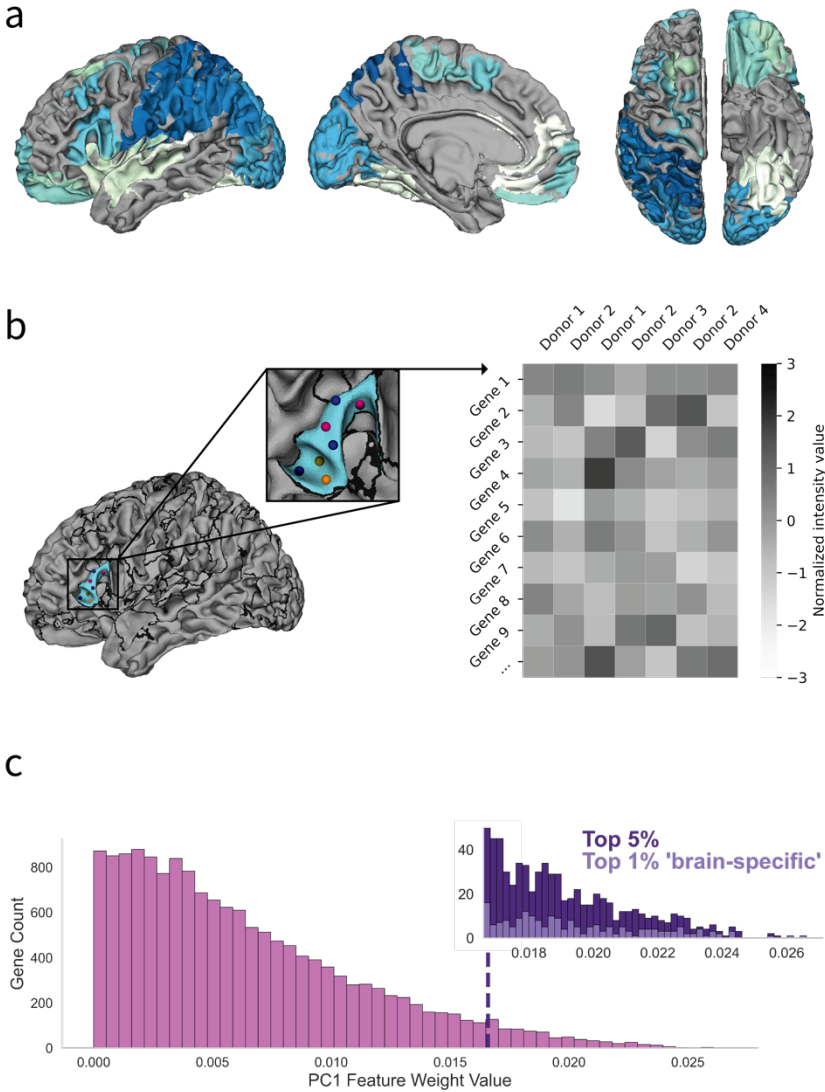
Fig. 1 Gene selection within cytoarchitectonic neighborhoods of the human cerebral cortex. **a** A recent, observer-independent approach (Amunts et al., 2020) parcellated the human cerebral cortex (HCC) into 111 cytoarchitectonic areas covering approximately 70% of the HCC (Materials and Methods). **b** Left: Each tissue sample from 6 post-mortem brains was aligned to this novel cytoarchitectonic parcellation (Materials and Methods). Example locations of several different probes from different donors are depicted within area 45 ("Broca's" area) within the inferior frontal cortex. Each color corresponds to a single donor, with each probe containing the relative intensity value of the microarray expression for the genes surveyed. Right: Matrix illustrating the transcriptomic data across the different probes within a single region. Each column corresponds to one of the probes shown on the left. Each row is the normalized expression value of a single gene. **c** A histogram

of the absolute value of feature weights for PC1 are shown (pink) along with the selection of the top 5% of genes with the highest feature weight values (dark purple). The top 200 genes that were most differentially expressed across all 111 cROIs were selected and used for the remainder of the analyses after filtering for 'brain-specific' genes (Burt et al., 2018).

Observer-independent cytoarchitectonic areas are embedded within two opposing transcriptomic gradients

As previous research showed that cROIs in the visual processing hierarchy are located within opposing transcriptomic gradients (Gomez et al. 2019), we tested the targeted hypothesis that this relationship extended more broadly to cROIs distributed throughout HCC. To test this hypothesis, the top 200 genes were submitted to an agglomerative hierarchical clustering algorithm (Materials and Methods), similar to the previously mentioned study. This approach revealed that genes clustered into two groups at the highest level with branch distances much greater than that of other clustering levels (Fig. 2a). These two clusters generated two opposing gradients among cROIs: one that increased in expression and another that decreased in expression along the order determined by score values from PC1 (Fig. 2b). Interestingly, however, only 20% of genes overlapped between the present group of genes and those identified previously that contributed to the positioning of areas in the visual processing hierarchy (Gomez et al. 2019). This large difference between gene sets, one connected to the organization of the visual hierarchy and the other connected to the whole HCC organization, may be due to regional differences in cellular diversity, cellular density, and even developmental origin.

We also tested the correlation between the hypothesis matrix and the observed matrix and found an R-value of 0.87 with a range of 0.74 to 0.92 (Fig. 2c) when randomly selecting for 50% of the cROIs (permuted N = 1,000). Furthermore, we generated a null distribution of

correlations between the hypothesis matrix and shuffled cROIs, which was well below the range observed for 50% of the ordered cROIs, indicating the robustness of the identified relationship. For comparison, we also applied the same clustering method, but to the bottom 200 genes, which revealed a much more homogenous and smaller branching distance across levels (Fig. 2a), further supporting that this relationship was specific to the genes most differentially expressed among cROIs distributed throughout the HCC.
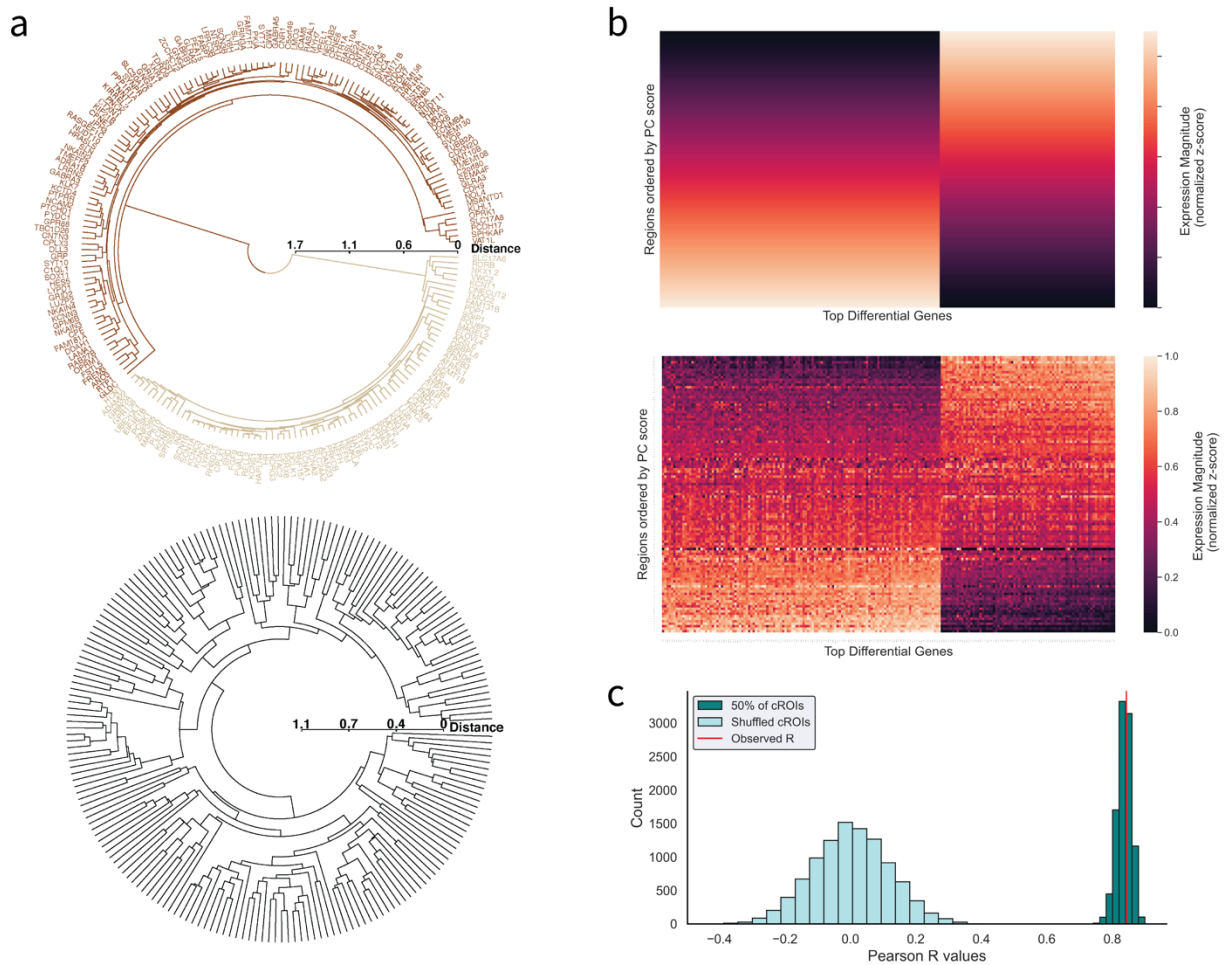

Fig. 2 Binary clustering of the top 200 genes reveals that opposing expression gradients contribute to the cytoarchitectonic layout of cortical areas identified using an observer-independent technique. **a** Dendrograms showing the algorithmic clustering of the top and bottom 200 genes. (top) The top 200 genes that are most

differentially expressed cluster predominantly into two groups at the highest level (brown and tan). The names of each gene are plotted radially. (bottom) On the contrary, hierarchical clustering reveals minimal distance between branches for the bottom 200 genes, indicating very little transcriptomic differences between clusters in the dendrogram. **b** (top) Hypothesis matrix of genetic gradients (based on Gomez et al., 2019). The hypothesis matrix was created using a stepwise change in gene expression for each cROI as ordered by their PC score in which one set increases, and the other set decreases, in expression across regions. (bottom) Observed matrix of the gene expression of the top 200 differentially expressed genes (y-axis) across the 111 cROIs ordered by their score from PC1 (x-axis). The brown cluster of genes from **a** represents the increasing cluster on the left, while the tan cluster from **a** represents the descending cluster on the right. **c** We calculated the correlation between the hypothesis matrix and the observed matrix by randomly selecting from 50% of the cROIs to correlate with corresponding rows in the hypothesis matrix and bootstrapped with an N=1,000. This resulted in a distribution of values ranging from 0.74 to 0.90 with an observed R value of 0.84 (p < 0.0001). We also generated a null distribution (N = 1,000; cyan) of R values by shuffling the cROI order in the observed matrix prior to correlating it to the hypothesis matrix.

Primary axis of transcriptomic variation reveals within and between network clustering of cytoarchitectonic areas

PCA on the cROIs with each gene set as a feature identified that the first PC explained 24.12% of the variance. As such, we refer to PC1 as a representation of the primary axis of transcriptomic variation in the cytoarchitectonic arealization of HCC. There is a clear structure among the distribution of cROIs along this primary axis: early visual areas were positioned on one end of the transcriptomic axis (Fig. 3a, hOc1 (e.g, striate cortex, or V1), hOc2 (V2), etc., lower right column), while frontal and insular regions were positioned on the other end of the axis (Fig. 3a, Ia2, Op7, etc; upper right column).

To further explore the relationship of this primary axis of transcriptomic variation to the arealization of the HCC, we generated transcriptomic profiles - or *fingerprints* (Fig. 3c) - for

17

each cROI consisting of the normalized average expression of the top 200 differentially expressed (DE) genes. Using these transcriptomic fingerprints, we then performed an agglomerative hierarchical clustering algorithm to examine the different clusters of cROIs based on the similarity of transcriptomic fingerprints. These similarities were further represented in a 2-dimensional plane using Multi-Dimensional Scaling (MDS) in which the Euclidean distance between regions represented the transcriptomic similarity or dissimilarity to other regions.

This analysis revealed two primary clusters of cROIs based on transcriptomic fingerprints. One cluster represented in orange in Fig. 3b primarily consists of regions from frontal, cingulate, and insular regions, while the other cluster represented in green contains regions from occipital, parietal, and temporal regions. Furthermore, within each cluster, there are smaller subdivisions (various shades of green and orange in Fig. 3b). When further exploring the clustering within the MDS, we found that there were two types of genetic similarities. One shows 'within transcriptomic network' clustering, such as visual regions that cluster together in the dark green cluster in the lower left of Fig. 3b. The other shows 'across transcriptomic network' clustering such as fusiform regions (FG1, FG2, FG3, and FG4). For example, even though both areas FG2 and FG4 (i) are located in the lateral FG, (ii) contain regions that are selective for faces and words, and (iii) are cortically adjacent to each other (Weiner et al. 2017), they are located within different transcriptomic networks. These qualitative differences can be observed in the transcriptomic fingerprints highlighted in Fig. 3c.

To test if spatial proximity contributed to transcriptomic similarity, we calculated the ratio between the pairwise Euclidean distance between two cROIs in the MDS plane and the corresponding geodesic distance on the surface (Fig. 3d). Both distance metrics were

normalized. Values in red (greater than 1) correspond to a greater transcriptomic difference over geodesic distance while values less than 1 (in blue) correspond to a greater geodesic distance than transcriptomic difference. Pairwise ratio values are shown for the 8 representative cROIs that were also illustrated in Fig. 3c. Ultimately, while there are a few cROIs that are as transcriptomically similar as they are proximal, for a majority of regions, geodesic distance does not determine transcriptomic similarity. For example, regions hOc1 and Area 1 are cortically far apart, but transcriptomically similar; however, regions FG1 and FG2 are cortically proximal to FG3 and FG4, but are transcriptomically distinct from each another. These observed relationships are consistent with the recent structural model (García-Cabezas et al. 2019), which proposes that macroanatomical organization is driven by factors such as connectivity, timing of development, and neural proliferation. Support for the structural model, in comparison to the distance rule model (Barbas, 1986), which postulates that anatomical similarity is due to distance between regions, has been established in both macaques and humans (Hilgetag et al. 2016; Beul et al. 2017; Zikopoulos et al. 2018; Aparicio-Rodríguez and García-Cabezas 2023).

For cROI 'across network clustering' pairs, we quantified the relationship between transcriptomic similarity and cortical distance by calculating a transformed ratio value (absolute value of the Pearson's correlation coefficient in gene expression between two regions divided by the normalized geodesic distance along the surface) and then subtracted this value from 1 (Supplementary Fig. 2a). 0 represents region pairs that are both highly correlated and cortically distant. The region pair to exhibit the strongest 'across network clustering' are regions 4p of the somatosensory cortex and Ph3 of the parahippocampal cortex (R = 0.81 and normalized geodesic distance = 0.77) that cluster together with early visual regions and other

somatosensory regions. Other surprising region pairs include STS2 in superior temporal cortex with p32 in medial anterior cingulate cortex, hOc3v in extrastriate visual cortex with 4a in primary motor cortex, and hOc1 in striate cortex with 3b in primary somatosensory cortex. The combination of these findings indicate that transcriptomic similarity between region pairs is not driven by cortical proximity.

Lastly, we repeated our analyses with a variable number of genes (N = 100, 500, 1,000 and 1,500) to test if the number of genes affected the clustering of regions. Compared to our analyses with 200 genes, we found that the clusters remain stable across the different Ns observed with decreasing Rand Index values as the number of genes increased (Fig. 3e). This finding further enhances the reliability of the clustering results.
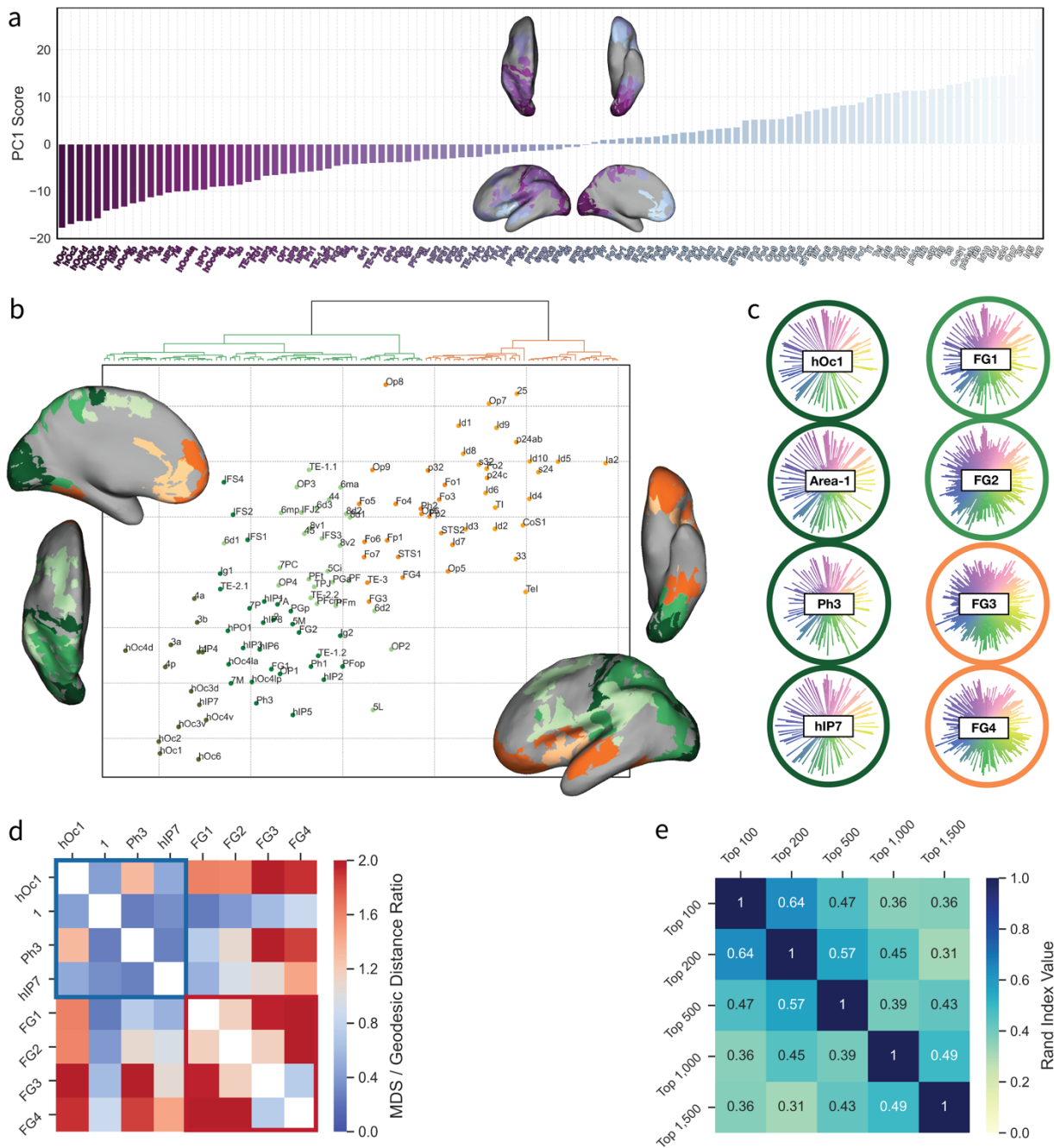
Fig. 3 Hierarchical clustering of transcriptomic fingerprints reveals within and between network clustering of cytoarchitectonic areas. **a** Scores obtained from the first PC, highlighting the linear order of cROIs that is used for visualizations in figures throughout the manuscript. Score values from the first PC (y-axis) are plotted as a function of each cROI (x-axis), ordered by score values (from lowest (left) to highest (right)). Names of the cROIs ordered by the first PC are illustrated on the bottom axis starting with hOc1 on the left in dark purple and ending with

insular region Ia2 in light blue on the far right. Also shown are topographic plots that illustrate the score value for the cROIs on the MNI152 inflated cortical surface. cROIs in dark purple have a lower PC score while cROIs in light purple have a higher PC score. **b** Agglomerative hierarchical clustering was applied to the cROIs and their expression of the 200 most differentially expressed genes, which revealed two main clusters (orange and green) at the highest level (top) with subclusters shown in different shades of green and orange. Topographical representations of the cROIs with their corresponding cluster label are also shown in different views. To further illustrate the genetic differences and similarities between cROIs, multidimensional scaling was applied to cROIs and their differential gene expression and then color-coded using labels from the hierarchical clustering. Regions close together in the 2-D plane are more transcriptomically similar and regions further apart are more transcriptomically dissimilar. Within the MDS, there are two main types of genetic similarities: within-network and between-network. For example, all the early visual regions cluster together in the dark green cluster on the left highlighting within-network similarities. Additionally, while regions FG1, FG2, FG3 and FG4 are cortically adjacent to one another, FG1 and FG2 are in one transcriptomic cluster (green), while FG3 and FG4 are in a transcriptomically distinct cluster (orange). The former areas cluster more closely to parietal areas, while the latter cluster more closely with areas in superior temporal cortex, both of which are indicative of between network clustering. **c** Transcriptomic fingerprints of selected cROIs in which the radial axis shows the relative gene expression for the top 200 differential genes. The column on the left highlights regions within the same cluster, while the column on the right highlights regions across two different clusters to qualitatively illustrate the similarities and differences in gene expression profiles. **d** Ratio comparison between geodesic distance of cROIs and their transcriptomic similarity as measured by the Euclidean distance between the cROIs on the MDS 2-D plane. Values in red (or above one) have a greater transcriptomic difference than geodesic distance (i.e. across network clustering) while values in blue (or less than one) have a greater geodesic distance than transcriptomic difference (i.e. within network clustering). **e** Rand index matrix representing the pairwise stability of cluster labels when selecting for a different number of the highest feature weight values (N = 100, 200, 500, 1,000 and 1,500 genes), while still limiting analyses to brain-specific genes (N =1,898).

Genes differentially expressed across a multimodal parcellation result in a similar clustering of regions

While the cytoarchitectonic parcellation covers most of the HCC (~70%), we also considered a multimodal parcellation with full coverage of the HCC (Glasser et al., 2016). With this parcellation, we repeated our previous analyses (see Material and Methods) using hierarchical clustering of multimodal ROIs based on their expression of the top 200 differentially expressed genes (Fig. 4). At the highest level, there are two broad clusters that have the same differentiation to the cytoarchitectonic parcellation, as well as additional sub-clustering with 'across-network' and 'within-network' features (Fig. 4a). Within the 2D Euclidean space, V1 and other early visual regions are at one end while insular regions are at the other end. Interestingly, many regions that are located in the 'gap maps' of the cytoarchitectonic parcellation tend to cluster with other frontal and insular regions with the exception of a few cingulate regions and temporal regions that cluster with more occipital and parietal regions.

Additionally, we tested how similar the differentially expressed gene sets were between the two parcellations (Fig. 4b). For the top 200 genes selected from each parcellation, 90% of the genes were the same, which is consistent with the similar clustering results across parcellations described above. This was replicated for each N iteration of genes (N = 100, 200, 500, and 1,000), which maintain similar distributions of overlap between gene sets.

Fig. 4 90% overlap of the top genes contributing to either cytoarchitectonic or multimodal parcellations of the

HCC. **a** Differential gene expression, clustering, and MDS analyses were also performed for AHBA data aligned to a recent multimodal parcellation of the HCC. Similarly to the cytoarchitectonic parcellation, there are two clusters at the highest level separating primary sensory regions from frontal and insular regions with similar subclusters shown in the lighter shades of green and orange. Also, similar results occur for the MDS analysis: V1 is at one end of the MDS axis, while insular regions are positioned at the other end. **b** Venn-diagrams represented as horizontal bars for the overlapping genes between the two different parcellations. Different rows correspond to the different sized N of top differential genes (N = 100, 200, 500, 1,000) that were 'brain-specific' (see Burt et al., 2018). For the top 200 differentially expressed genes, 180 of the 200 genes overlap and the other 20 genes are unique to each parcellation. Through each iteration of N genes, at least 8% of genes are unique to either parcellation with the most being 14%.

CT/M ratio: A combined metric that is highly correlated with the primary axis of transcriptomic variation

What underlying anatomical features are related to this primary axis of transcriptomic variation? While previous research has explored the relationship between transcriptomics and continuous gradients of cortical thickness and myelination individually (Burt et al. 2018), our results show that (1) these transcriptomic clusters are more strongly correlated with a combined metric of cortical thickness and myelination, as well as other anatomical features and (2) the striate cortex and primary motor cortex are very transcriptomically similar to one another. This is somewhat surprising since striate cortex is cortically thin, heavily myelinated, cell dense, and has a prominent and subdivided layer IV (Collins et al. 2010; Balaram and Kaas 2014; Gomez et al. 2021), while primary motor cortex is cortically thick, heavily myelinated, relatively cell sparse (compared to striate cortex) and the presence and prominence of layer IV is contentious (García-Cabezas and Barbas 2014; Barbas and García-Cabezas 2015).

Given recent work showing that the ratio between cortical thickness and myelination

(CT/M ratio) was a particularly useful metric for parcellating one HCC area from another (Willbrand et al. 2022), we hypothesized that despite these differences in anatomical and architectonic features across cortical areas, transcriptomic similarities may be capturing a ratio of anatomical features. To test this hypothesis, we aligned our cROIs to average cortical thickness and myelination maps from the 1,096 participants included in the Human Connectome Project (HCP). This analysis revealed a strong positive correlation between the expression of these 200 genes and the CT/M ratio across cROIs of the HCC as shown in Fig. 5a ($R=0.872$; $p < 0.01e^{-34}$). We also repeated the PCA analysis and CT/M measurements in individual donor brains and found that for most donors, the correlation remained high between the PC1 score of regions and CT/M. Variations across donors is likely due to the variability in probe coverage and differences in alignment between the template cytoarchitectonic atlas and donor-specific volume space.

In addition to this CT/M ratio, underlying cytoarchitectonic features likely contributing to this primary transcriptomic axis are cell density and the presence/prominence of layer IV. For example, striate cortex (lower left of Fig. 5a) has a uniquely prominent layer IV with several sublayers, as well as is the most cell dense area in the HCC (Collins et al. 2010; Balaram and Kaas 2014; Gomez et al. 2021). Additionally, visual areas have a higher cell density than HCC areas outside of visual cortex (Collins et al. 2010). Further, area Ia2 does not have a layer IV (agranular) while areas Id5 and OP7 have a thin layer IV (von Economo 2009; Zilles and Amunts 2012; Amunts and Zilles 2015) (dysgranular; upper right of Fig. 4a). Thus, to further test if there was also a relationship between cell density, granularity, and the primary axis of transcriptomic variation of the cROIs, we incorporated cell density and layer IV thickness estimates from the classic Von Economo - Koskinas atlas into our computational,

multimodal pipeline (Materials and Methods). This analysis showed a negative correlation (R =

-0.579, $p < 2.90e^{-11}$) between cell density and the primary axis of transcriptomic variation (Fig.

5b). Layer IV thickness was also negatively correlated with the primary axis of transcriptomic

variation (R = -0.428, $p < 6.21e^{-6}$; Fig. 5c). Altogether, the primary axis of transcriptomic

variation among cROIs likely reflects aspects of cell density, the presence/prominence of layer
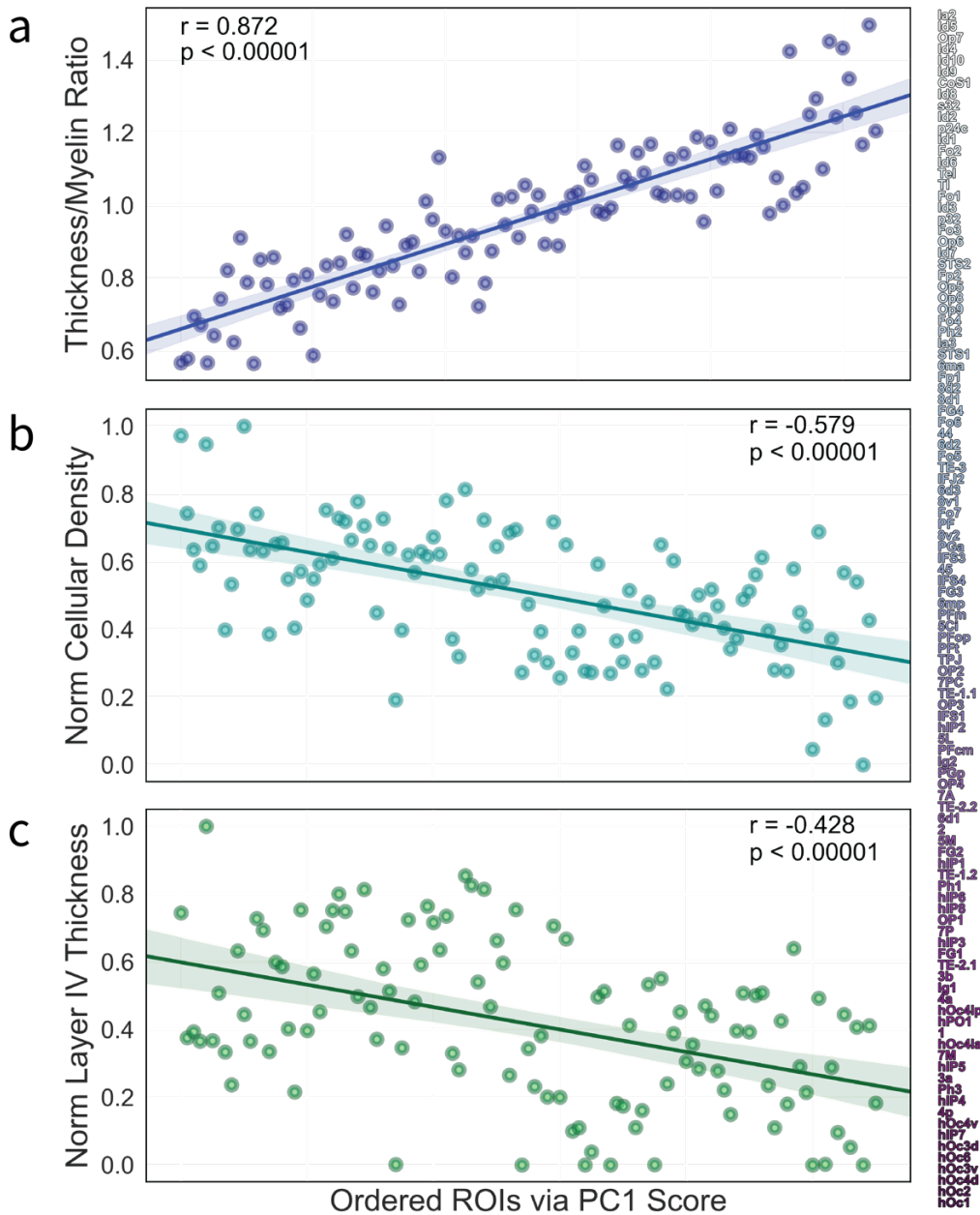
IV, and the CT/M ratio.

Fig. 5 The CT/M ratio, cell density, and layer IV thickness correlate with the primary axis of transcriptomic variation. **a** The CT/M ratio as a function of PC score. There is a strong positive correlation between the two metrics (Pearson's R = 0.872, $p < 0.01e^{-34}$). **b** Normalized cell density (y-axis) is negatively correlated with PC score for each cROI (x-axis; Pearson's R = -0.579, $p < 2.90e^{-11}$)). **c** Normalized layer IV thickness (y-axis) is negatively correlated with PC score for each cROI (x-axis; Pearson's R = -0.428, $p < 6.21e^{-6}$).
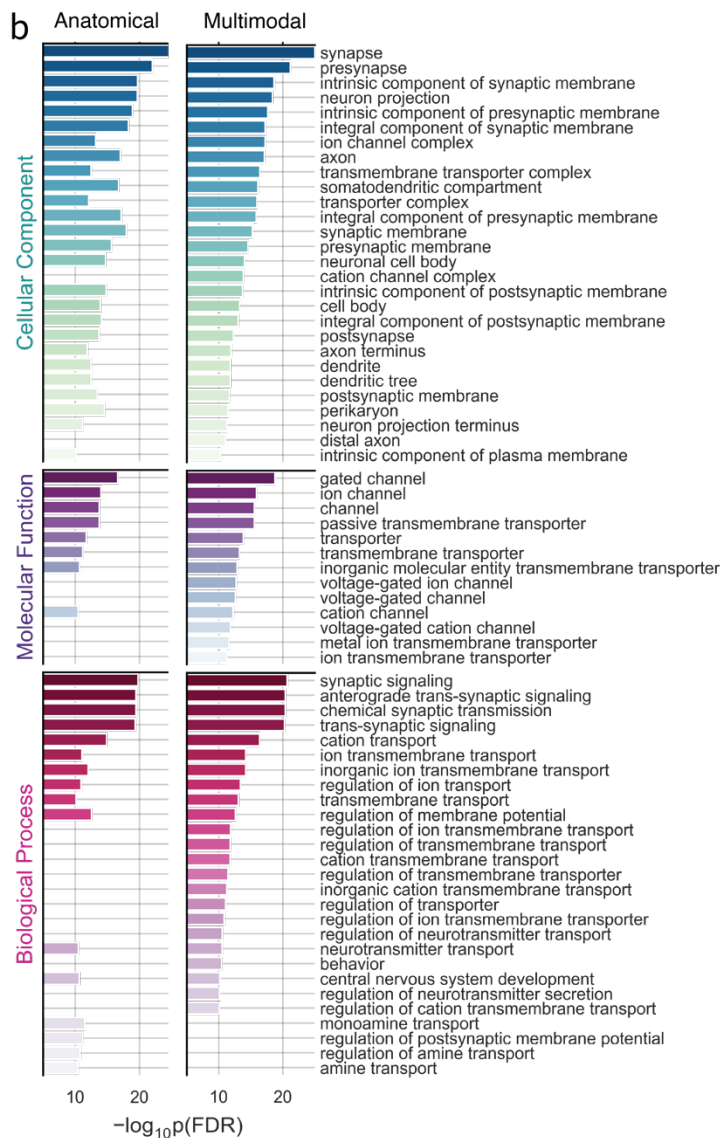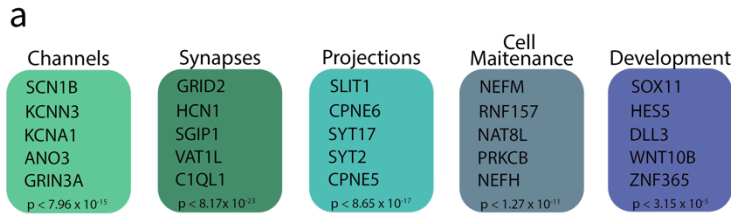
Gene enrichment analyses reveal that different sets of genes contribute to cytoarchitectonic and multimodal HCC parcellations

To gain a deeper understanding of the functional roles of the top 200 differentially expressed genes contributing to the observer-independent cytoarchitectonic parcellation of the HCC, gene symbols were submitted to an enrichment analysis resulting in five clusters of unique structural or functional properties (Materials and Methods). The most significant terms were associated with channel and synaptic function, cellular projections and maintenance, and transport of molecules or ions (Fig. 6a).

To test if these genes were specific to the cytoarchitectonic parcellation of the HCC or generalized to additional parcellations of the HCC, we repeated our analyses with a multimodal parcellation of the HCC (Glasser et al., 2016; Fig. 4a). Our quantifications revealed that roughly 90% of the top 200 genes are shared between parcellation modality, while roughly 10% are different. Specifically, we repeated the enrichment analyses with different sized sets of differential genes (N=100, N=200, N=500, N=1,000; Fig. 4b). Through each iteration, at least 8% of genes are unique to either parcellation with the most being 14%.
Interestingly, enrichment analyses showed that parcellation-specific genes had different functions: cytoarchitectonic arealization genes were enriched in molecular functions such as transmembrane transport activity and ion channel activity while the multimodal arealization

genes were enriched in functions such as calcium channel activity and cellular processes such as neuron development (Fig. 6b). Furthermore, we submitted the top 200 differentially expressed genes of the cytoarchitectonic parcellation to a protein-protein network analysis via the STRING database (Supplemental Fig. 9). We found that the most connected network of genes performed ion-channel functions and belonged to the KCNA and SCN family, while the second most connected network consisted of neurotransmitter-related genes followed by cell maintenance genes.

Fig. 6 Cytoarchitectonic genes are more enriched in cell body functions and amine transport, while *multimodal genes* are more enriched in ion channel and transport functions. **a** List of 5 key annotation categories (along with example genes associated with each category from the Gene Ontology (GO) Database) for the 180 genes overlapping between the cytoarchitectonic parcellation and the multimodal parcellation (Fig. 4). Top categories

include ion channel function, synaptic function, cellular projections, cell maintenance, and brain development. **b** Gene enrichment results for the differing sets of genes for the cytoarchitectonic (left column) and multimodal (right column) parcellation of the HCC. Each GO term is plotted by the log-transformed FDR-corrected p-value in the horizontal bars for their respective significance in either set of genes (i.e. cytoarchitectonic or multimodal). Given that 180 of the genes are the same between both sets, enrichment results are similar for each set in which both are heavily enriched in synaptic functions. Yet, differences between the two sets show that the 'anatomical' gene set is more enriched in cell body functions and amine transport while the 'multimodal' genes are more enriched in ion channel and transport functions.

Discussion

In the present study, we implemented a data-driven approach and identified transcriptomic contributions to a modern algorithmic cytoarchitectonic parcellation of the HCC. These findings provide a clear bridge to recent parallel empirical tracks examining the contributory role of transcriptomics to identified gradients and maps of the HCC. The first track explores the relationship between transcriptomics and gradients in the HCC (Burt et al. 2018; Gomez et al. 2019; Vogel et al. 2022). The second track explores the relationship between transcriptomic-based parcellations (TBP) of the HCC relative to modern and classic areal parcellations of the HCC (Gryglewski et al. 2018, 2022; Shine et al. 2022). The ~~first~~ bridge is that neither track considered a modern, observer-independent cytoarchitectonic parcellation of the HCC – instead, they considered observer-dependent parcellations that have several shortcomings as discussed previously (Amunts and Zilles 2015; Amunts et al. 2020). The results provided by the present study integrate these two empirical tracks in a critical manner and provide theoretical insights for future studies. Below, we discuss these findings in the context of: i) the role of transcriptomics, cortical thickness, and myelination for integrating continuous gradients and discrete, classic "crazy-pavement maps" along a modern "cortical

spectrum," ii) transcriptomics as a bridge connecting areas of functionally distinct cortical networks, and iii) transcriptomics contributing to different scales of organization and different parcellations of the HCC.

The role of transcriptomics, cortical thickness, and myelination for integrating continuous gradients and discrete, classic "crazy-pavement maps" along a modern "cortical spectrum"

In the broader neurology, cognitive neuroscience, and human brain mapping communities, the last decades continue a longstanding trend of identifying gradients and parcellations of the HCC. For example, in a review of Bailey and Bonin's *Isocortex of Man*, Le Gros Clark (1952) wrote: "Finally, neurologists should continue to regard with the greatest suspicion the incredibly complicated "crazy-pavement" maps of cortical areas which have from time to time been elaborated by the Vogt school since Campbell's and Brodmann's original studies were first published" (Le Gros Clark 1952). Both Brodmann and Sanides (among others) were students of the "Vogt school" and along with the Vogts, produced a parcellation of the HCC into ~180-200 areas over several decades (Nieuwenhuys 2013; Foit et al. 2022) – a number that is comparable to maps produced with modern multimodal and data-driven methods (Huth et al. 2016; Glasser et al. 2016). Despite this "crazy-pavement" map, the Vogts (Vogt and Vogt 1919) also acknowledged that the boundaries among adjacent cortical areas were not sharp and building on their hypothesis, Sanides (Sanides 1964) proposed that in addition to cortical areas, there were directions of "gradation" streams that correlated with directions of brain evolution and neocortical development (summarized by (Henssen et al. 2016).

A recent study (John et al. 2022) proposed the concept of a *cortical spectrum* that builds on the foundation of this classic work by integrating three features of functional and structural organization: i) a mosaic of functionally and structurally distinct parcellations of the cortical mantle, ii) a seemingly heterogenous six-layered structure in which connectivity is the driving factor of functional differences (Barbas 1986; Barbas and Rempel-Clower 1997), and iii) gradients of architectonic structure that predict cortico-cortical connections. Here, we propose that our results nicely complement and extend these classic and modern theoretical and empirical findings linking different scales of brain structure and function by incorporating the correlated relationship between gene expression and the CT/M ratio, in which there is a stronger relationship with gene expression than either cortical thickness or myelination alone (Supplemental Fig. 6).

Specifically, the primary axis of transcriptomic variation as captured by PCA identified in the present study is strongly associated with the granularity, or lamination, of cROIs. For example, highly granular regions, such as hOc1 (primary visual cortex) and 4a (a subarea of primary motor cortex), appear together on one end of the spectrum while more dysgranular or agranular regions, such as many insular and frontal cROIs in limbic cortices, appear on the other end (Fig. 5). This complements findings that have been found previously in the mouse neocortex (Fulcher et al. 2019), as well as previous results of a hierarchy of transcriptomic specialization of the human and primate neocortex. Specifically, Burt and colleagues (2018) refer to an anatomical hierarchy as "a globally self-consistent ordering of cortical areas according to characteristic laminar patterns of interareal projections." While the laminar patterns of interareal projections have not been demonstrated for the recently identified human cROIs explored here (though see recent work of the *structural model* proposed by (García-

Cabezas et al. 2019), the present findings show that similar stages of a hierarchy can be transcriptomically dissociable. For example, even though areas FG1 and FG2 are cortically adjacent to one another in the posterior fusiform gyrus and presumably at a similar stage of the visual processing hierarchy, FG1 is more transcriptomically similar to OP1 in the parietal operculum than FG2, which is more transcriptomically similar to area 5M in medial parietal cortex and PGp in lateral parietal cortex. The present findings are also consistent with the *cortical spectrum* proposal, as well as two recent transcriptomic findings in three main ways.

First, John and colleagues (2022) implemented a data driven approach and identified a *cortical spectrum* of weakly laminated areas on one end and sharply laminated areas on the other end broadly across the cortex, but within lobes as well – in which the degree of lamination contributes to cortical *types*. While their results were based on quantitative assessments of histology and immunochemistry, as well as MR data in non-human primates, our results identify that transcriptomics play a role in this potential *cortical spectrum* and that the CT/M ratio serves as a useful metric in relating the balance between continuous gradients and discrete regions. For example, John and colleagues (2022) write: "Cortical types must be understood as discretizations of these continuous gradients." We propose that the CT/M ratio serves as a metric bridging the gap between continuous gradients and discretized parcellations.

Second and third, respectively, these findings also complement recent studies reporting *transcriptomic distinctiveness* (Wagstyl et al. 2022) with visual cortex on one end and frontal cortex on the other in addition to a genetic variation along a *sensorimotor-association (S-A) cortical axis (Sydnor et al. 2021)*, which has also been associated with the distribution of transmitter receptors (Goulas et al. 2021). Many terms aside – from *crazy-pavement* classically to *cortical spectrum* and *transcriptomic distinctiveness* modernly – altogether the present

findings incorporate the CT/M ratio as a feature that can guide future studies striving to build mechanistic models to better understand the relationship among gradients, areal parcellations, and cortico-cortical connectomics, as well as the role of transcriptomics and the CT/M ratio as metrics mediating this complex relationship of brain structure, function, cortical networks, and genetic expression.

Transcriptomics as a bridge connecting areas of functionally distinct cortical networks

While previous findings show that transcriptomics contribute to the arealization of a cortical network specialized for visual processing (Gomez et al. 2019), the present findings also show that areas located in different functional networks can also be more transcriptomically similar to one another than areas located in the same functional network. Specifically, even though visual areas also cluster together in the present study (lower left in Fig. 3b), a subset of visual areas are also transcriptomically similar to areas in somatomotor cortices (3a,3b,4a,4b), secondary somatosensory cortex (OP1), and posterior parietal cortex (hiP3, hiP5, hiP6).

Additionally, even though Ph1 and Ph2 are adjacent to one another in parahippocampal cortex, the data-driven approach implemented here situates them in distinct transcriptomic clusters with different functions: Ph1 is transcriptomically similar to areas in auditory cortex, the parietal operculum, and posterior parietal cortex, while Ph2 is transcriptomically similar to areas in orbitofrontal cortex. While there are many other examples, the combination of these findings indicate two main points. First, despite being located in different functional networks, cortical areas may also be transcriptomically similar and share a common function despite being commonly associated to one cortical network. Second, while a large portion of the transcriptomic landscape across the cortical sheet exhibits a high degree of spatial

autocorrelation where nearby anatomical regions have more similar patterns of gene expression than distal regions (Burt et al. 2020), the genes identified here that exhibit the greatest degree of differential expression show that cortical distance is not the primary indicator of transcriptomic similarity (Fig. 3d). Instead, a likely anatomical feature underlying genetic similarity between cortically distant regions in addition to those measured here is white matter connectivity – especially so given that previous studies (Arnatkeviciute et al. 2021c) have found a high degree of transcriptomic coupling between long-range connectivity hubs over local, short-range connections. This is further supported by work done in both the human and macaque PFC, showing that white matter systematically varies with grey matter in which strongly interconnected regions tend to have similar laminar structures (Zikopoulos et al. 2018). Findings from our work and others would also suggest similar transcriptomics profiles.

Another possible explanation that would link systematic variation in grey matter, white matter, and gene expression would be the developmental origin of cortical regions. For instance, Nieuwenhuys and Puelles (Nieuwenhuys and Puelles 2015) proposed parcellating the HCC into fundamental morphological units (FMUs) that separates regions based on their embryological origin. In a broader review of multiple parcellations of the primate thalamus, including functional, cyto-, myelo-, and geno-architecture based parcellations, Garcia-Cabezas and colleagues (2023) further suggest that differential expression of certain genes across the neural plate give rise to different cortical 'types', which they refer to as the 'onto-phylo neuroanatomy' paradigm. Taken together, a goal for future studies will be to determine what anatomical, functional, developmental, and even evolutionary features contribute to the intriguing finding that cytoarchitectonic areas can be cortically distant from one another and assigned to different functional networks, and yet, transcriptomically similar to one another.

Transcriptomics contribute to different scales of organization and different parcellations of the HCC

The combination of findings across studies indicate that different sets of genes contribute to different scales of functional or anatomical organization. For example, while a sparse set of genes contribute the most variance to gradients of the HCC (Burt et al. 2018) at a meso-scale, maps within a single cortical area at the fine-scale (Gomez et al. 2021), and the parcellation of the HCC into distinct cortical areas at the macro-scale (present study), largely distinct sets of genes contribute to each type of organization. Together, these findings show that transcriptomics contribute to different scales of organization of the HCC. But, what about different functional roles of different sets of genes at the same level? For example, at the macro-scale considering different parcellations of the HCC (cytoarchitectonic vs. multimodal)? In the present study, our data-driven analysis approach showed that roughly 10% (or 8-14% if choosing different sets of genes; Fig. 4b) of the identified genes were different between the cytoarchitectonic and multimodal parcellation. Furthermore, enrichment analyses showed that genes specific to a cytoarchitectonic parcellation were generally more related to cell maintenance functions that likely contribute to the cellular scaffolding necessary for cytoarchitectonic features. On the other hand, genes specific to a multimodal parcellation were more associated with ion channel and transport functions, which may be related to features related to neural activation – a component contributing to the borders of the multimodal atlas (Glasser et al. 2016). In terms of limitations, a factor that could contribute to these differences is ROI size: cytoarchitectonic ROIs tend to be larger than multimodal ROIs. However, when looking at the genes that overlap between the two parcellations, both sets are heavily enriched

in synaptic function, furthering the relevance of differential expression to cell-to-cell interactions.

Nevertheless, an additional limitation of the present study is that the analyses were conducted in brains from healthy elderly adults. Thus, a goal of future studies is to test whether the genes identified here also contribute to the transcriptional landscape of the developing human brain.

Conclusion

Using a data-driven approach, we tested and found that a sparse subset of genes differentially contributed to a modern cytoarchitectonic parcellation of the HCC. The expression of this sparse subset of genes was correlated with the CT/M ratio, a metric that bridges the gap among i) gradients at the macroscale, ii) areas at the meso-scale, and iii) cell density at the microscale. The combination of these findings not only influences future studies examining transcriptomic contributions to the recent models and theories discussed here (i.e., cortical spectrum, structural model, etc.), but also developmental and evolutionary (i.e. onto-phylo neuroanatomy paradigm) contributions to the multimodal relationship identified across spatial scales in the present study.

Funding

Acknowledgements

Competing Interests

All authors declare that no competing interests exist.

Data Availability

All original datasets used are publicly available (see *Materials and Methods*) and the code need to replicate the analyses will be made freely accessible upon publication.

References

Abbott A (2003) Neuroscience: A new atlas of the brain. Nature 424:249–250. https://doi.org/10.1038/424249a

Amunts K, Mohlberg H, Bludau S, Zilles K (2020) Julich-Brain: A 3D probabilistic atlas of the human brain's cytoarchitecture. Science 369:988–992

Amunts K, Zilles K (2015) Architectonic Mapping of the Human Brain beyond Brodmann. Neuron 88:1086–1107. https://doi.org/10.1016/j.neuron.2015.12.001

Aparicio-Rodríguez G, García-Cabezas MÁ (2023) Comparison of the predictive power of two models of cortico-cortical connections in primates: the distance rule model and the structural model. Cereb Cortex 33:8131–8149. https://doi.org/10.1093/cercor/bhad104

Armstrong E, Schleicher A, Omran H, et al (1995) The ontogeny of human gyrification. Cereb Cortex 5:56–63. https://doi.org/10.1093/cercor/5.1.56

Arnatkeviciute A, Fulcher BD, Bellgrove MA (2021a) Imaging transcriptomics of brain disorders. Psychiatry Global Open …

Arnatkeviciute A, Fulcher BD, Bellgrove MA, Fornito A (2021b) Where the genome meets the connectome: Understanding how genes shape human brain connectivity. Neuroimage 244:118570. https://doi.org/10.1016/j.neuroimage.2021.118570

Arnatkeviciute A, Fulcher BD, Fornito A (2019) A practical guide to linking brain-wide gene expression and neuroimaging data. Neuroimage 189:353–367. https://doi.org/10.1016/j.neuroimage.2019.01.011

Arnatkeviciute A, Fulcher BD, Oldham S, et al (2021c) Genetic influences on hub connectivity of the human connectome. Nat Commun 12:4237. https://doi.org/10.1038/s41467-021-24306-2

Balaram P, Kaas JH (2014) Towards a unified scheme of cortical lamination for primary visual cortex across primates: insights from NeuN and VGLUT2 immunoreactivity. Front Neuroanat 8:81. https://doi.org/10.3389/fnana.2014.00081

Barbas H (1986) Pattern in the laminar origin of corticocortical connections. J Comp Neurol 252:415–422. https://doi.org/10.1002/cne.902520310

Barbas H, García-Cabezas MÁ (2015) Motor cortex layer 4: less is more. Trends Neurosci 38:259–261. https://doi.org/10.1016/j.tins.2015.03.005

Barbas H, Rempel-Clower N (1997) Cortical structure predicts the pattern of corticocortical connections. Cereb Cortex 7:635–646. https://doi.org/10.1093/cercor/7.7.635

Beul SF, Barbas H, Hilgetag CC (2017) A Predictive Structural Model of the Primate Connectome. Sci Rep 7:43176. https://doi.org/10.1038/srep43176

Bludau S, Mühleisen TW, Eickhoff SB, et al (2018) Integration of transcriptomic and cytoarchitectonic data implicates a role for MAOA and TAC1 in the limbic-cortical network. Brain Struct Funct 223:2335–2342. https://doi.org/10.1007/s00429-018-1620-6

Brodmann K (1909) Vergleichende Lokalisationslehre der Grosshirnrinde in ihren Prinzipien dargestellt auf Grund des Zellenbaues. Barth

Burt JB, Demirtaş M, Eckner WJ, et al (2018) Hierarchy of transcriptomic specialization across

human cortex captured by structural neuroimaging topography. Nat Neurosci 21:1251–1259. https://doi.org/10.1038/s41593-018-0195-0

Burt JB, Helmer M, Shinn M, et al (2020) Generative modeling of brain maps with spatial autocorrelation. Neuroimage 220:117038. https://doi.org/10.1016/j.neuroimage.2020.117038

Chen J, Bardes EE, Aronow BJ, Jegga AG (2009) ToppGene Suite for gene list enrichment analysis and candidate gene prioritization. Nucleic Acids Res 37:W305–11. https://doi.org/10.1093/nar/gkp427

Collins CE, Airey DC, Young NA, et al (2010) Neuron densities vary across and within cortical areas in primates. Proceedings of the National Academy of Sciences 107:15927–15932. https://doi.org/10.1073/pnas.1010356107

Deco G, Kringelbach ML, Arnatkeviciute A, et al (2021) Dynamical consequences of regional heterogeneity in the brain's transcriptional landscape. Science Advances 7:eabf4752

Fischl B (2012) FreeSurfer. Neuroimage 62:774–781. https://doi.org/10.1016/j.neuroimage.2012.01.021

Fischl B, Sereno MI, Dale AM (1999) Cortical surface-based analysis. II: Inflation, flattening, and a surface-based coordinate system. Neuroimage 9:195–207. https://doi.org/10.1006/nimg.1998.0396

Foit NA, Yung S, Lee HM, et al (2022) A whole-brain 3D myeloarchitectonic atlas: Mapping the Vogt-Vogt legacy to the cortical surface. Neuroimage 263:119617.

https://doi.org/10.1016/j.neuroimage.2022.119617

Fornito A, Arnatkevičiūtė A, Fulcher BD (2019) Bridging the Gap between Connectome and

Transcriptome. Trends Cogn Sci 23:34–50. https://doi.org/10.1016/j.tics.2018.10.005

Fulcher BD, Murray JD, Zerbi V, Wang X-J (2019) Multimodal gradients across mouse cortex.

Proc Natl Acad Sci U S A 116:4689–4695. https://doi.org/10.1073/pnas.1814144116

García-Cabezas MÁ, Barbas H (2014) Area 4 has layer IV in adult primates. Eur J Neurosci

39:1824–1834. https://doi.org/10.1111/ejn.12585

García-Cabezas MÁ, Pérez-Santos I, Cavada C (2023) Mapping the primate thalamus: historical

perspective and modern approaches for defining nuclei. Brain Struct Funct 228:1125–1151.

https://doi.org/10.1007/s00429-022-02598-4

García-Cabezas MÁ, Zikopoulos B, Barbas H (2019) The Structural Model: a theory linking

connections, plasticity, pathology, development and evolution of the cerebral cortex. Brain

Struct Funct 224:985–1008. https://doi.org/10.1007/s00429-019-01841-9

Glasser MF, Coalson TS, Robinson EC, et al (2016) A multi-modal parcellation of human

cerebral cortex. Nature 536:171–178. https://doi.org/10.1038/nature18933

Gomez J, Zhen Z, Weiner KS (2019) Human visual cortex is organized along two genetically

opposed hierarchical gradients with unique developmental and evolutionary origins. PLoS

Biol 17:e3000362. https://doi.org/10.1371/journal.pbio.3000362

Gomez J, Zhen Z, Weiner KS (2021) The relationship between transcription and eccentricity in

human V1. Brain Struct Funct 226:2807–2818. https://doi.org/10.1007/s00429-021-02387-5

Goulas A, Changeux J-P, Wagstyl K, et al (2021) The natural axis of transmitter receptor

distribution in the human cerebral cortex. Proc Natl Acad Sci U S A 118.:

https://doi.org/10.1073/pnas.2020574118

Gryglewski G, Murgaš M, Klöbl M, et al (2022) Enrichment of Disease-Associated Genes in

Cortical Areas Defined by Transcriptome-Based Parcellation. Biol Psychiatry Cogn

Neurosci Neuroimaging 7:10–23. https://doi.org/10.1016/j.bpsc.2021.02.012

Gryglewski G, Seiger R, James GM, et al (2018) Spatial analysis and high resolution mapping of

the human whole-brain transcriptome for integrative analysis in neuroimaging. Neuroimage

176:259–267. https://doi.org/10.1016/j.neuroimage.2018.04.068

Hawrylycz MJ, Lein ES, Guillozet-Bongaarts AL, et al (2012) An anatomically comprehensive

atlas of the adult human brain transcriptome. Nature 489:391–399.

https://doi.org/10.1038/nature11405

Henssen A, Zilles K, Palomero-Gallagher N, et al (2016) Cytoarchitecture and probability maps

of the human medial orbitofrontal cortex. Cortex 75:87–112.

https://doi.org/10.1016/j.cortex.2015.11.006

Hilgetag CC, Medalla M, Beul SF, Barbas H (2016) The primate connectome in context:

Principles of connections of the cortical visual system. Neuroimage 134:685–702.

https://doi.org/10.1016/j.neuroimage.2016.04.017

Huth AG, de Heer WA, Griffiths TL, et al (2016) Natural speech reveals the semantic maps that

tile human cerebral cortex. Nature 532:453–458. https://doi.org/10.1038/nature17637

John YJ, Zikopoulos B, García-Cabezas MÁ, Barbas H (2022) The cortical spectrum: A robust

structural continuum in primate cerebral cortex revealed by histological staining and

magnetic resonance imaging. Front Neuroanat 16:897237.

https://doi.org/10.3389/fnana.2022.897237

Le Gros Clark WE (1952) A Note on Cortical Cyto-architectonics. In: Isocortex of Man. pp 96–

104

Marcus DS, Harwell J, Olsen T, et al (2011) Informatics and data mining tools and strategies for

the human connectome project. Front Neuroinform 5:4.

https://doi.org/10.3389/fninf.2011.00004

Markello RD, Arnatkeviciute A, Poline J-B, et al (2021) Standardizing workflows in imaging

transcriptomics with the abagen toolbox. Elife 10.: https://doi.org/10.7554/eLife.72129

Nieuwenhuys R (2013) The myeloarchitectonic studies on the human cerebral cortex of the

Vogt-Vogt school, and their significance for the interpretation of functional neuroimaging

data. Brain Struct Funct 218:303–352. https://doi.org/10.1007/s00429-012-0460-z

Nieuwenhuys R, Puelles L (2015) Towards a New Neuromorphology. Springer

Oldham S, Fulcher BD, Aquino K, et al (2022) Modeling spatial, developmental, physiological,

and topological constraints on human brain connectivity. Sci Adv 8:eabm6127.

https://doi.org/10.1126/sciadv.abm6127

Sanides F (1964) Structure and function of the human frontal lobe. Neuropsychologia 2:209–

219. https://doi.org/10.1016/0028-3932(64)90005-3

Scholtens LH, de Reus MA, de Lange SC, et al (2018) An MRI Von Economo - Koskinas atlas. Neuroimage 170:249–256. https://doi.org/10.1016/j.neuroimage.2016.12.069

Seidlitz J, Nadig A, Liu S, et al (2020) Transcriptomic and cellular decoding of regional brain vulnerability to neurogenetic disorders. Nat Commun 11:3358. https://doi.org/10.1038/s41467-020-17051-5

Shine JM, Arnatkeviciute A, Fornito A, Fulcher BD (2022) Navigating a Complex Landscape: Using Transcriptomics to Parcellate the Human Cortex. Biol Psychiatry Cogn Neurosci Neuroimaging 7:3–4

Sydnor VJ, Larsen B, Bassett DS, et al (2021) Neurodevelopment of the association cortices: Patterns, mechanisms, and implications for psychopathology. Neuron. https://doi.org/10.1016/j.neuron.2021.06.016

Vogel JW, Alexander-Bloch A, Wagstyl K, et al (2022) Conserved whole-brain spatiomolecular gradients shape adult brain functional organization. bioRxiv 2022.09.18.508425

Vogt C, Vogt O (1919) Allgemeine Ergebnisse unserer Hirnforschung. J.A. Barth

von Economo C (2009) Cellular Structure of the Human Cerebral Cortex. Karger Medical and Scientific Publishers

von Economo CF, Koskinas GN (1925) Die Cytoarchitektonik der Hirnrinde des erwachsenen Menschen. J. Springer

Wagstyl K, Adler S, Seidlitz J, et al (2022) Transcriptional Cartography Integrates Multiscale Biology of the Human Cortex. bioRxiv 2022.06.13.495984

Wang Y, Royer J, Park B-Y, et al (2022) Long-range functional connections mirror and link microarchitectural and cognitive hierarchies in the human brain. Cereb Cortex. https://doi.org/10.1093/cercor/bhac172

Weiner KS, Barnett MA, Lorenz S, et al (2017) The Cytoarchitecture of Domain-specific Regions in Human High-level Visual Cortex. Cereb Cortex 27:146–161. https://doi.org/10.1093/cercor/bhw361

Welker W (1990) Why Does Cerebral Cortex Fissure and Fold? In: Jones EG, Peters A (eds) Cerebral Cortex: Comparative Structure and Evolution of Cerebral Cortex, Part II. Springer US, Boston, MA, pp 3–136

Willbrand EH, Voorhies WI, Yao JK, et al (2022) Presence or absence of a prefrontal sulcus is linked to reasoning performance during child development. Brain Struct Funct 227:2543–2551. https://doi.org/10.1007/s00429-022-02539-1

Zachlod D, Bludau S, Cichon S, et al (2022) Combined analysis of cytoarchitectonic, molecular and transcriptomic patterns reveal differences in brain organization across human functional brain systems. Neuroimage 257:119286. https://doi.org/10.1016/j.neuroimage.2022.119286

Zikopoulos B, García-Cabezas MÁ, Barbas H (2018) Parallel trends in cortical gray and white matter architecture and connections in primates allow fine study of pathways in humans and reveal network disruptions in autism. PLoS Biol 16:e2004559. https://doi.org/10.1371/journal.pbio.2004559

Zilles K (2018) Brodmann: a pioneer of human brain mapping-his impact on concepts of cortical organization. Brain 141:3262–3278. https://doi.org/10.1093/brain/awy273

Zilles K, Amunts K (2010) Centenary of Brodmann's map — conception and fate. Nat Rev Neurosci 11:139–145. https://doi.org/10.1038/nrn2776

Zilles K, Amunts K (2012) Architecture of the Cerebral Cortex. The Human Nervous System 836–895